PCCP

View Online
Dynamic Article Links

Cite this: *Phys. Chem. Chem. Phys.*, 2011, **13**, 14318–14324

www.rsc.org/pccp

PAPER

Electron-beam evaporated silicon as a top contact for molecular electronic device fabrication†

Rajesh Kumar,[a] Haijun Yan,[b] Richard L. McCreery[ab] and Adam Johan Bergren*[b]

Received 14th March 2011, Accepted 1st June 2011
DOI: 10.1039/c1cp20755e

This paper discusses the electronic properties of molecular devices made using covalently bonded molecular layers on carbon surfaces with evaporated silicon top contacts. The Cu "top contact" of previously reported carbon/molecule/Cu devices was replaced with e-beam deposited Si in order to avoid Cu oxidation or electromigration, and provide further insight into electron transport mechanisms. The fabrication and characterization of the devices is detailed, including a spectroscopic assessment of the molecular layer integrity after top contact deposition. The electronic, optical, and structural properties of the evaporated Si films are assessed in order to determine the optical gap, work function, and film structure, and show that the electron beam evaporated Si films are amorphous and have suitable conductivity for molecular junction fabrication. The electronic characteristics of Si top contact molecular junctions made using different molecular layer structures and thicknesses are used to evaluate electron transport in these devices. Finally, carbon/molecule/silicon devices are compared to analogous carbon/molecule/metal junctions and the possible factors that control the conductance of molecular devices with differing contact materials are discussed.

1. Introduction

Charge transport across nanoscopic molecular layers has been studied using a variety of experimental paradigms.[1–6] In contrast to studies using spectroscopic measurements of bridge-mediated donor/acceptor systems[5] or measurements of the redox kinetics at chemically modified electrodes,[7–10] a molecular electronic junction usually relies on direct electrode-to-molecule contacts to make a complete electronic circuit.[1,2,4,11–20] The incorporation of a molecular component directly into a solid state device enables fundamental studies into the parameters that control charge transport across molecules and also opens several avenues in the quest for next-generation electronic devices.

The fabrication of a molecular junction is often carried out using bottom-up approaches. First, a conductive surface is modified with a nanoscopic organic layer, often based on self-assembled monolayers. Next, the circuit is completed by depositing conducting contacts onto the top of the molecular layer. Numerous methods for top contact deposition have been employed, including the direct evaporation of metals onto the layer[1,11,21–23] and more complex procedures that seek to minimize perturbing the molecules in the organic layer.[17,24] Central in many of these cases is how the contacts influence the electronic behaviour of the finished junction.[25] The chemical, physical, and electronic properties of the contact material can impact the response of the device, as can interactions of the molecular layer with the contacts, including possibly destructive or structure-altering forces.

Several methods have been developed to circumvent disrupting the structure of the molecular layer, including the use of conductive polymer top contacts,[24] liquid metals,[26–29] and other techniques.[17] We have been exploring the use of an alternative method for making molecular junctions utilizing conductive carbon films with diazonium-derived molecular layers.[1,11,23,29–31] Direct deposition of copper metal onto the top of the molecular layers in a cross-bar format produces large area ($\sim$0.4 $\times$ 0.4 mm) junctions that have high yield (90% or greater) and are reproducible (the relative standard deviation, or RSD, of the current density at 0.1 V is $<$ 15%).[1,11] The very flat conducting carbon substrate (with a root mean square, or rms, roughness of $<$ 0.5 nm) and the strong covalent C–C bond between the substrate and molecular layer result in good reproducibility and thermal tolerance. The integrity of the molecular layer after metal deposition has been verified spectroscopically,[32,33] and completed devices can be cycled between 5 and 450 K without significant changes in electronic behaviour.[1] The electronic properties of the carbon/molecule/Cu devices made with direct Cu deposition are very similar to those made with a "soft" surface diffusion-based

[a] *Department of Chemistry, University of Alberta, Edmonton, Alberta, Canada*
[b] *National Institute for Nanotechnology, Edmonton, Alberta, Canada. E-mail: Adam.Bergren@nrc.ca; Fax: 780 641 1601; Tel: 780 641 1762*

† Electronic supplementary information (ESI) available: Additional characterizations and electronic measurements. See DOI: 10.1039/c1cp20755e

deposition method.[31] Transport in such junctions is consistent with quantum mechanical tunnelling through a barrier defined by the offset between the contact Fermi level and the molecular HOMO.[1]

Although carbon/molecule/Cu molecular junctions exhibit reproducible electronic behaviour consistent with tunnelling, metals are often problematic in microelectronics due to potential oxidation or electromigration.[34] The industry often uses "covalent conductors" such as titanium nitride and Ti/W alloys as conductors in microelectronic circuits to avoid such problems.

The current paper outlines experiments investigating electron-beam deposited silicon (e-Si) films to replace Cu as the top contact in molecular junctions. Si is covalent and does not migrate in high electric fields, and its distinct electronic properties compared to Cu may provide further insight into electron transport mechanisms. The e-Si is characterized using conductivity measurements, UV/vis and Raman spectroscopy, and other techniques. The electronic characteristics of carbon/molecule/Si/Au junctions are evaluated as a function of molecular structure and thickness, and over a range of temperatures (77–400 K). Although numerous investigations have been reported using crystalline Si as a substrate in molecular electronics (a recent and excellent review is available),[16] the disordered e-Si films used here should have substantially different properties. With this in mind, we compare the electronic characteristics of the e-Si top contact devices with that for Cu and comment on the possible causes for the observed differences in conductivity. Finally, we outline possible consequences of the use of e-Si in the quest to understand the parameters that control charge transport in molecular electronic junctions.

2. Experimental

The bottom-up approach for fabricating molecular junctions follows our earlier reports,[1,11,23,30] but uses Si as a top contact. Patterned pyrolyzed photoresist films (PPF) are produced on an insulating substrate (thermally oxidized Si wafers or polished quartz) by standard lithographic patterning of photoresist into 0.5 mm lines. After patterning, the photoresist is pyrolyzed by heating to 1100 °C under a constant flow of 5% H_2 in N_2, holding for 1 h, and cooling to room temperature. PPF is structurally and electronically similar to glassy carbon, which has been used in electrochemistry for several decades.[35–37] PPF has a lower density of electronic states than a metal, but no band gaps, and a resistivity of ~0.006 Ω-cm.[35,37,38] The PPF surface is disordered but very flat (typically < 0.5 nm rms roughness over a 10 × 10 μm area), and very uniform molecular layers may be formed on PPF by diazonium reduction.[38]

Deposition of aromatic molecular layers onto PPF is carried out by the electrochemical reduction of diazonium reagents, as described elsewhere.[1] In addition, the oxidation of aliphatic amines was used to deposit alkane-based molecular layers as described recently.[39] Molecules used to construct electronic junctions include azobenzene (AB), nitroazobenzene (NAB), and octylamine. Since both methods for depositing molecular layers can result in multilayers, molecular layer thicknesses were measured using an AFM "scratching" method.[38] To complete the junction, 30 nm Si (0.99999 pure) and 20 nm Au (0.9999 pure) were deposited sequentially *via* electron beam evaporation through shadow masks oriented in perpendicular lines ~0.4 mm in width. The pressure during deposition was ~5 × 10^{-6} Torr and the deposition rate was ~0.1 nm s^{-1}). Junction areas measured after fabrication are ~0.0012 to 0.0017 cm^2, depending on the particular shadow mask used to deposit the top contact.

Raman spectroscopy was carried out using a custom-built spectrometer that is described elsewhere[40] or a Thermo/Nicolet Raman microscope. Optically transparent PPF[41,42] (OTPPF) used in backside Raman[32,33,43] is made by pyrolysis of diluted photoresist (5% v/v in propylene glycol methyl ether acetate) on quartz (Q) substrates. A molecular layer of NAB, which has a very strong Raman scattering profile,[44] was deposited using reduction of the diazonium precursor onto the Q/OTPPF sample. Finally, half of this sample was masked using aluminium foil and 30 nm of Si was deposited onto the un-masked surface. Raman spectra were then collected through the substrate in both Si-coated and non-coated areas.

DC electrical measurements were carried out using 4-wire mode with either a Keithley 2602A or a custom-built LabView (National Instruments) measurement system immediately after removing the devices from the evaporation chamber in order to obtain consistent results. Device conductance is observed to decrease with time (see supplemental information Fig. S-1 and associated discussion). In all cases the drive voltage is placed on the PPF and the *J–V* curves plot the voltage of the PPF *versus* the top contact.[45]

3. Results and discussion

In order to investigate any structural changes to the molecular layer caused by the direct evaporation of top contact materials, we have developed techniques to probe the molecular structure at a buried interface using Raman spectroscopy.[32,33] Fig. 1 shows an overlay of Raman spectra for a molecular layer of NAB on optically transparent PPF, obtained through the substrate, without (black curve) and with (red curve) a 30 nm layer of evaporated Si. These spectra were both obtained from the same sample through the ~50% transparent PPF substrate. The black spectrum was obtained from an area that was masked from Si deposition while the red spectrum was obtained from an

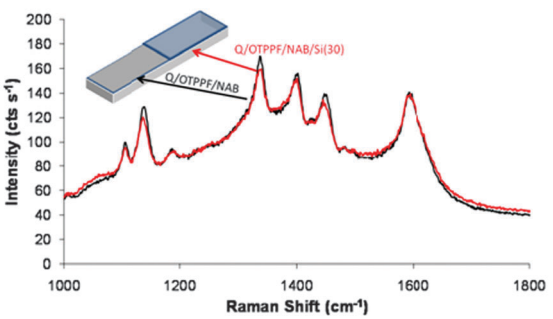

Fig. 1 Raman spectra for NAB chemisorbed on optically transparent PPF (OTPPF) obtained through the substrate without (black curve) and with (red curve) a 30 nm layer of Si deposited *via* direct electron beam evaporation.

area coated with 30 nm Si (the same thickness used in the fabrication of junctions). Notably, the signature for NAB is observed after direct deposition of Si, with no significant changes in the intensities or ratio of intensities of any of the Raman bands (Table S-1 in the supplementary information lists peak assignments for the Raman bands of NAB). Similar results were obtained when a 40 nm layer of metal (Al) was evaporated on top of the 30 nm Si layer without breaking vacuum. These results indicate that NAB survives the direct deposition of Si with no detectable changes in its molecular structure.

Fig. 2 shows the average current density-voltage (J–V) curves for several junctions of PPF/AB(3.8)/Si(30)/Au(20) (numbers in parenthesis are thicknesses in nm) from two different chips (see Fig. S-2 in the supplemental information for an overlay of all 8 junctions from each chip). Typically, 3 or 4 out of 4 tested devices on a chip yielded non-shorted and stable J–V curves, and overall yields (where a working device is defined as a non-shorted junction with a stable, non-linear J-V curve) were quite high, exceeding 90% for the 68 devices tested during this study (see Table S-2 in supplemental information). The RSD in Fig. 2 is below 30% throughout the entire voltage range. This junction-to-junction variation is similar to our recent reports using Cu metal as a top contact.[1] In addition, the batch-to-batch variation in current density is typically within a factor of $\sim$2 (see supplemental information Fig. S-3, which shows overlays of J–V curves from five different batches), which is also similar to our previous reports using Cu metal top contacts.[11] This level of variation can be expected based on the spatial distribution of the tunnel distance across the junction[46] taking into account the level of roughness of the contacts ($<$0.5 nm) and the averaging of J across the large area of these junctions. The general shape of the J–V curves for the e-Si top contact devices are similar to that for the Cu top contact devices, although the current magnitude is significantly lower (as discussed in more detail below).

It is important to note that the J–V curves for PPF/molecule/Si devices are approximately symmetric at all bias values. Analysis of Fig. 2 yields rectification ratios (*i.e.*, the quotient of the absolute values of J for positive bias to negative bias) of 1.6 at 3 V. Transport controlled by a metal/semiconductor interface can either be ohmic or rectifying, and the level of symmetry shown in Fig. 2 indicates that the e-Si films make non-rectifying contacts. In addition, this result also indicates the lack of a significant Schottky barrier between the e-Si and Au film, which is consistent with an amorphous Si layer lacking a well-defined band structure. These results imply that the e-Si film can be treated as a conductive medium for making contact to molecular layers. Although the symmetry indicates that the molecular layer may control the transport, the properties of the e-Si film may still impact the overall conductance of the junction through a variety of mechanisms. In order to de-convolute the role played by the molecular component and the contacts, we have fabricated a series of junctions containing different molecular layer thicknesses and structures, used different e-Si thicknesses, measured J–V curves as a function of temperature, and assessed various properties of the e-Si film. Analysis of these disparate effects on junction conductance permits determination of a "molecular signature" relating structure to conductance.

Fig. 3 shows a series of J–V curves for PPF/AB/Si devices with different molecular layer thicknesses. The current density decreases exponentially with thickness (see Fig. S-4 in the supplemental information), indicating that quantum mechanical tunneling is a likely transport mechanism. The attenuation factor (β) determined from this figure is 2.3 nm^{-1}, while a series of junctions containing NAB molecules yielded 2.5 nm^{-1}(see Fig. S-5 in the supplemental information for NAB data). These values are consistent with previous measurements of β for transport across conjugated, diazonium-derived molecular layers using a variety of methods. For example, in molecular junctions similar to those reported here but with Cu metal top contacts,[1] β for these molecules was 2.5 nm^{-1} for both AB and NAB. Electron transport measurements carried out using a redox couple in solution at carbon electrodes modified with biphenyl and nitrobiphenyl[47] yielded β = 2.2 nm^{-1}. The good agreement between the attenuation factors for the different junctions implies a

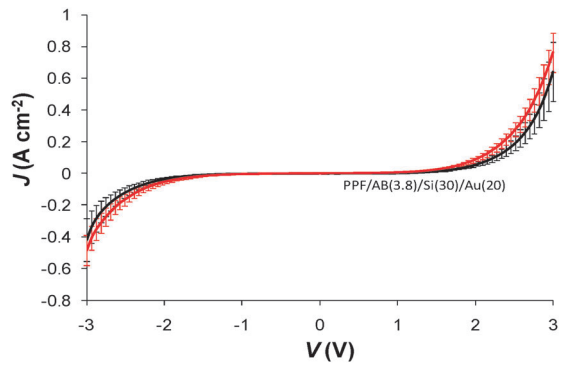

Fig. 2 Average J–V curves with error bars representing the standard deviation of J for two different chips of PPF/AB(3.8)/Si(30)/Au(20). The numbers in parenthesis indicate film thicknesses in nm. The black curve represents 4 devices on a single chip, while the red curve is for 3 devices on a second chip.

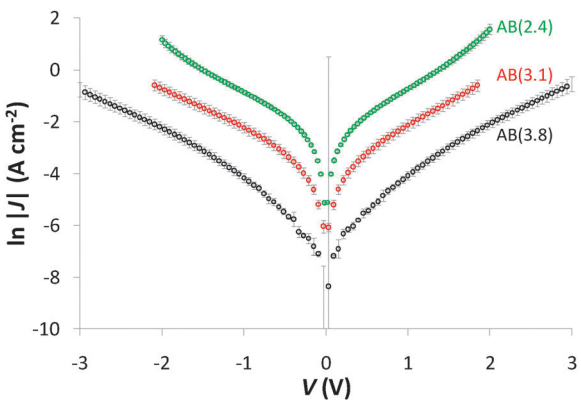

Fig. 3 J–V curves for a series of azobenzene (AB) junctions with different molecular layer thicknesses using 30 nm Si and 20 nm Au as the top contact. Each plot is the average of four junctions with the ln-scale standard deviation represented by error bars (*i.e.*, the error bars are the magnitude of the relative error σ/J_{avg}). The attenuation factor calculated from this data is 2.3 $\pm$ 0.1 nm^{-1} (see Fig. S-4 in the supplementary information).

common transport mechanism. Furthermore, it serves as one indication that transport in the PPF/molecule/Si devices reported here is substantially influenced by the molecular component.

Several possible electron transport mechanisms are strongly temperature dependent, while others have weak T-dependence.[48] Fig. 4 shows an Arrhenius plot for an e-Si top contact molecular junction containing a 3.8 nm layer of AB obtained over the range from 100 to 400 K (see supplemental information Fig. S-6 for an additional Arrhenius plot for a different junction). J increased less than 30% for this temperature range, yielding an Arrhenius slope of $\sim$8 meV for temperatures above 200 K, and $\sim$1.5 meV for lower temperatures. These apparent barriers are small compared to most molecular rearrangements or reactions, and are consistent with a tunneling mechanism. Although the small increase in J with temperature might have a variety of origins, the slight increase in current at higher temperature is consistent with the effect of temperature on the carrier distribution around the Fermi level of the contacts, as discussed recently.[1] In any case, the results in Fig. 4 indicate that quantum mechanical tunneling is likely the primary charge transport mechanism, similar to previously reported junctions with Cu top contacts[1] and implying a common transport mechanism.

To test if the e-Si film plays a role in limiting the conductance of the junctions, the thickness of the e-Si was varied while keeping the other parameters constant. Fig. 5 shows a series of three J–V curves for a 3.8 nm layer of AB with different thickness of e-Si (in all cases, 20 nm of Au was deposited onto the e-Si). The J–V curves in Fig. 5 show no difference for the different e-Si layer thicknesses tested. This result further indicates that the e-Si film serves as a conductive layer that makes ohmic contact with the molecules and that the electrical characteristics of the junction depend mainly on the molecular layer.

The results in Fig. 3–5 indicate that quantum mechanical tunneling is a likely mechanism for charge transport across the molecular layers. In order to determine limits for the contribution of the e-Si to junction conductance, we have assessed various electronic characteristics of e-Si alone made with the same e-beam process. Using a 4-point probe, the resistivity of a 30 nm e-Si film on quartz at room temperature was 3300 $\pm$ 300 Ω cm (the resistivity values varied from 2879 to

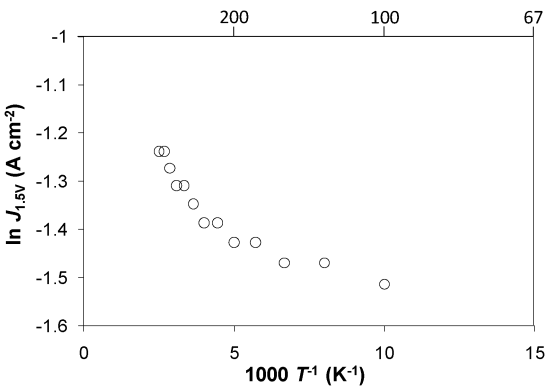

Fig. 4 Arrhenius plot for PPF/AB(3.8)/Si(30)/Au(20) junction. The value of the Arrhenius slope above 200 K (5 on the 1000 T^{-1} scale) corresponds to a "barrier" value of 8 meV.

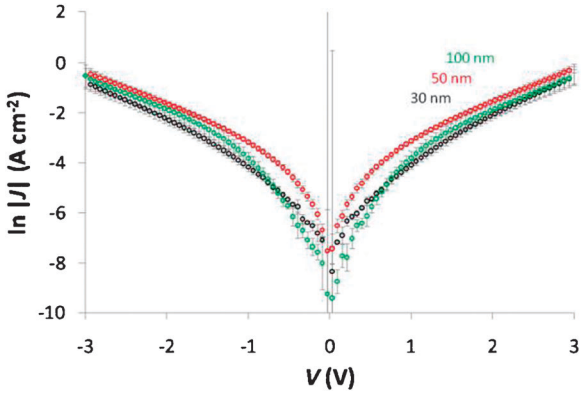

Fig. 5 J–V curves for a series of junctions with a 3.8 nm layer of azobenzene (AB) and three thickness of e-Si. A 20 nm layer of Au was deposited onto the e-Si in all cases. Error bars represent $\pm$ one standard deviation (scaled properly for a natural log).

3840 for different positions on different samples, but the average obtained for several positions on several samples was quite consistent). When translated to the expected resistance of a wire with a 0.0012 cm^2 cross sectional area (a typical junction area) a value of 8.25 Ω is obtained for a 30 nm length. The low-voltage junction resistance values (obtained by evaluating the inverse slope in the range of $\pm$ 0.1 V) in Fig. 5 are $\sim$100 kΩ, while those in Fig. 3 range from 2.7 to 95 kΩ for molecule-containing junctions. The magnitudes of these different resistance values illustrate that the conductance of the e-Si itself is sufficient to obtain molecule-controlled electrical measurements if a 4-wire mode is used to eliminate lead resistance. In addition, the extrapolated contact resistance, from a plot of the natural log of junction resistance (determined at low voltage) *vs.* thickness, is 4.8 Ω (see Fig. S-4B in the supplemental information). These results indicate that contact resistance does not significantly contribute to the measured junction conductance. Thus, variation of the molecular structure should result in electronic characteristics that reflect some aspect of the molecular component.

The identity of the molecular layer can impact a molecular junction through several factors. First, the molecular energy levels, often simplified by considering the frontier orbital energies, are clearly dependent on structure. The tunnelling barrier is often taken as the offset between the contact Fermi level(s) and the closest molecular energy level (usually the HOMO or LUMO, see Scheme 1). In this situation and with adequately thin layer thicknesses, charge carriers can be transported across the molecular layer through a non-resonant quantum mechanical tunneling mechanism. Second, electronic coupling between the molecular layer and the contact materials can influence the conductance of the junction. Third, the dielectric constant, effective carrier mass, and perhaps other parameters may also depend on molecular structure. While we will not attempt a systematic study of these factors here, we have fabricated molecular junctions using a structurally distinct set of molecules to compare to the aromatic layers discussed so far.

Alkane layers are often used to make molecular junctions,[4,18,49] with a value for β reported to be $\sim$10 nm^{-1}. Thus, alkanes represent a good test of molecular signature in a junction.

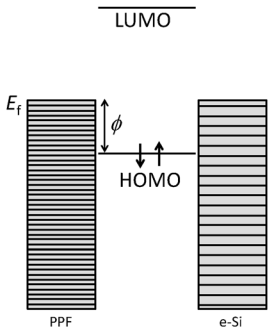

Scheme 1 Simplified energy level diagram showing the barrier for hole tunneling resulting from the offset between the contact Fermi level and the molecular HOMO. As shown in Table S-3 in supplemental information, different molecules will have different HOMO energies and this can explain, in part, the differences in conductance as a function of structure. The horizontal lines in the contacts represent the continuous density of states in the both the PPF and e-Si, which are both lower in magnitude that a typical metal.

Fig. 6 shows *J–V* curves for junctions with three different thicknesses of octyl amine molecular layers. An attenuation plot (see supplemental information Fig. S-7) gives $\beta \sim 9.9\ nm^{-1}$, which is reasonable given similar reported values for alkane-containing junctions measured in a variety of formats.[18] In addition, a comparison of junctions made using similar thicknesses of an aromatic or aliphatic layer made at the same time shows that the junction containing the saturated molecule is 4–8 times less conducting than that containing an aromatic azobenzene layer (see supplemental information Fig. S-8).

Scheme 1 shows a simplified energy level diagram that illustrates the formation of a tunneling barrier (ϕ) for holes due to the offset between the contact Fermi level and the molecular HOMO (*i.e.*, $\phi = E_f - E_{HOMO}$). The values for molecular HOMO and LUMO levels are compiled in supplemental information Table S-3, calculated using Gaussian '03[50] DFT (B3LYP) with a 6-31G(d) basis set, along with $E_f - E_{HOMO}$ values. Analysis of these data show that the barrier for AB (derived from gas-phase monomers) is expected to be $\sim$0.1 eV lower than that for the octyl amine, and therefore a higher current is expected for the AB junction, matching the observation. However, we note that this simplified picture does not take into account several important factors that can also determine the magnitude of *J* and the shape of the *J–V* curve. For example, we recently outlined an adaptation of the Simmons tunneling model for molecular junctions that takes into account several parameters that impact the tunnel barrier shape, and found that as the length of aromatic molecules increase,[1] many of these parameters change due to the delocalized nature of the electronic orbitals in aromatic structures. Thus, the values of the dielectric constant, effective carrier mass, and perhaps other parameters that impact the barrier shape can be expected to depend on the extent of electronic delocalization within the molecular component, which is substantial (and length dependent) for aromatic structures but negligible in the case of aliphatic molecules. The dynamic nature of the barrier shape for aromatic molecular junctions and the relative static picture for aliphatics impacts the values of β obtained as well as the overall conductance that is observed for a given junction.

Fig. 7 shows a plot of *J–V* curves for junctions with similar thicknesses of NAB, but using different top contact materials. All of the curves show a symmetric response with similar shapes. However, the conductances of the Cu junctions are much higher than that for the Si device, even though the thickness of one of the Cu devices is larger than that for the Si device. For example, at +0.5 V, the conductance of the Cu top contact devices is a factor of $\sim$240 (for the 4.5 nm NAB layer) or $\sim$20 (for the 3.3 nm NAB layer) times more than that for a 3.8 nm layer of NAB with an e-Si top contact. The example shown in Fig. 7 presents a clear case where the conductance must be analyzed by considering the junction in its entirety. Clearly, some property or properties of the top contact have a large impact on overall junction conductance. However, due to the large number of factors that can influence a molecular junction, the main contribution(s) to these changes is not easily identified. In other words, the overall performance of a molecular junction is not only controlled by the type of molecule but also by the layers involved in finishing the device. In the present case, the e-Si film is not affecting the thickness dependence of quantum tunnelling through molecular junctions but is playing some role in determining the overall conductance of the device.

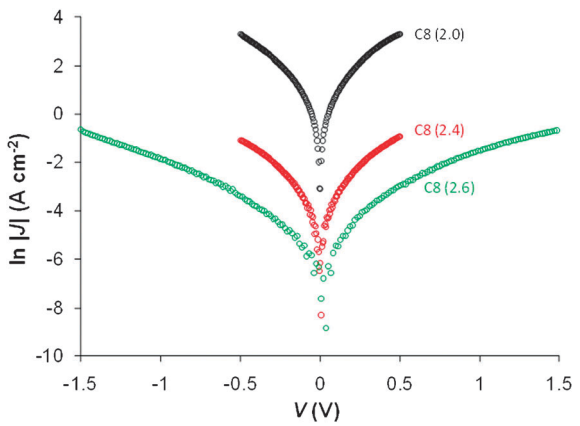

Fig. 6 *J–V* curves for junctions made using octylamine with three different thicknesses, where $\beta = 9.9\ nm^{-1}$.

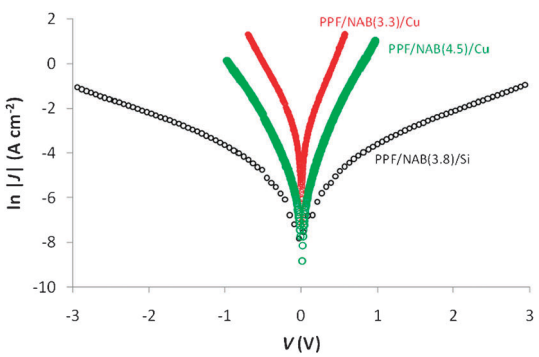

Fig. 7 *J–V* curves for junctions containing NAB with e-Si or Cu top contacts. The Cu devices, which were reported recently[1] are more conductive than the e-Si devices, even when the molecular layer thickness is larger.

As discussed earlier, the mechanism for charge transport in the junctions considered here is likely tunneling[1] and this probably applies to all of the junctions in Fig. 7. Often, the tunneling barrier for a molecular junction is approximated by considering the offset between the Fermi level in the contacts and one or more molecular orbitals (quite often this is simplified by considering the frontier orbitals). In order to determine if this simple model can explain the results in Fig. 7, we have measured several properties of the e-Si films.

Raman spectroscopy was used to determine disorder in the e-Si film. Raman spectra shown in the supplemental information (Fig. S-9) indicate that our as-deposited e-Si films are amorphous, with no indication of crystallinity. This is supported by UV-vis characterization (Fig. S-11), which shows an optical gap of $\sim$1.1 eV, but no features that show any distinguishable crystalline film structure. Finally, Fig. S-12 of the supplemental information shows a Kelvin probe measurement of a PPF surface coated with a 30 nm e-Si film, where the measured work function decreases from 5.0 eV for the uncoated PPF area to 4.2 eV for the area with the e-Si film. From these observations and previous characterizations[39] of the work function of various films measured by Kelvin probe, we find that the work function of the PPF is 5.0 eV, that for e-beam deposited Cu is 4.7 eV, and that for e-Si is 4.2 eV. The Simmons model used for PPF/molecule/Cu junctions,[1] predicts that a barrier height increase from $\sim$1.1 eV to $\sim$5 eV is required to explain the difference in conductance apparent in Fig. 7. Clearly the measured work function changes alone are not sufficient to explain Fig. 7, indicating that other differences between Cu and e-Si must affect junction conductance.

The electron carrier density of Si ($\sim 10^{10}$ cm^{-3}) is much lower than that for Cu ($\sim 10^{20}$ cm^{-3}): this is reflected in the much higher (*i.e.*, more than 9 orders of magnitude) resistivity values for our e-Si films compared to reported values for Cu.[51] This can influence the conductivity of the junction by making fewer carriers available for tunneling across the molecular layer in the case of e-Si. Thus, the apparent two orders of magnitude lower conductance for the e-Si films may be an effect of the lower carrier density. Along these same lines, the density of states of the material could play a similar role, although in this case the origin of the lower conductance would be rooted in fewer available states for the carrier to tunnel into (a subtle, but possibly important difference). Finally, other factors, such as interfacial electronic coupling, could be contributing to the difference in conduction between e-Si and Cu top contact devices.

Conclusions

We have presented a method for fabricating molecular junctions using electron beam evaporated Si as a top contact. The electrical characteristics of junctions containing both aliphatic and aromatic molecular layers of variable thickness were described, and the impact of molecular structure on the conductance of the junctions was evaluated. In addition, temperature dependent change in junction conductance was used to investigate the charge transport mechanism. The exponential variation of junction conductance with molecular layer thickness and the relative independence of junction current over a 100–400 K temperature range are consistent with quantum mechanical tunneling across the molecular layer. For the aromatic molecular layers, despite having an apparently similar charge transport mechanism (*i.e.*, similar β values and temperature dependence) to junctions with Cu metal top contacts, the overall current is much lower for the devices made with e-Si. Although we cannot currently determine the origin of this difference, we can conclude that a molecular junction must be considered as a system, together with the contacts, in order to fully understand all the factors that determine the current. Thus, although the e-Si films can be considered as a conductor that makes ohmic contact to the molecular layers used in this study, there are a variety of parameters that may influence the conductance of the device. Possible factors that can influence the devices made with e-Si include, but are not limited to: a lower carrier density or density of states (possibly a manifestation of the low conductance of the e-Si film compared to Cu), a low level of electronic coupling between the Si and the molecular layers, and a lower mobility for the charge carriers in the e-Si film, which is reflected in the lower number of carriers able to tunnel across the molecular layer. In addition, the fact that e-Si is a covalent conductor should significantly reduce problems with oxidation or electromigration of metallic contacts.

The influence of the molecular layer on junction conductance when using e-Si films was clearly demonstrated by the variation in junction behaviour with molecular structure and thickness. However, it is also apparent that the e-Si significantly affects the magnitude of the junction conductance. There are a variety of possible experiments that may help to answer some of the questions raised by these results. In addition, by controlling the properties of the Si film (*e.g.*, by doping it either during or after deposition), it may also be possible to probe the effect of other parameters that may be important in determining junction conductance (*e.g.*, charge carrier sign and mobility). In any case, the use of e-Si films in the fabrication of molecular electronic junctions will be a valuable tool for investigations of transport mechanisms and possibly in the design of functional electronic devices that incorporate molecular components.

Acknowledgements

This work was supported by The National Institute for Nanotechnology, The University of Alberta, and the MicroSystems Technology Research Initiative. The National Institute for Nanotechnology is operated as a partnership between the National Research Council and the University of Alberta and is jointly funded by the Government of Canada, the Government of Alberta, and the University of Alberta.

References

1 A. J. Bergren, R. L. McCreery, S. R. Stoyanov, S. Gusarov and A. Kovalenko, *J. Phys. Chem. C*, 2010, **114**, 15806–15815.
2 R. L. McCreery and A. J. Bergren, *Adv. Mater.*, 2009, **21**, 4303–4322.
3 D. M. Adams, L. Brus, C. E. D. Chidsey, S. Creager, C. Creutz, C. R. Kagan, P. V. Kamat, M. Lieberman, S. Lindsay, R. A. Marcus, R. M. Metzger, M. E. Michel-Beyerle, J. R. Miller,

M. D. Newton, D. R. Rolison, O. Sankey, K. S. Schanze, J. Yardley and X. Zhu, *J. Phys. Chem. B*, 2003, **107**, 6668–6697.
4 Y. Selzer and D. L. Allara, *Annu. Rev. Phys. Chem.*, 2006, **57**, 593–623.
5 P. P. Edwards, H. B. Gray, M. T. J. Lodge and R. J. P. Williams, *Angew. Chem., Int. Ed.*, 2008, **47**, 6758–6765.
6 E. H. Huisman, C. M. Guedon, B. J. van Wees and S. J. van der Molen, *Nano Lett.*, 2009, **9**, 3909–3913.
7 G. A. Edwards, A. J. Bergren, E. J. Cox and M. D. Porter, *J. Electroanal. Chem.*, 2008, **622**, 193–203.
8 A. J. Bergren and M. D. Porter, *J. Electroanal. Chem.*, 2005, **585**, 172–180.
9 A. J. Bergren and M. D. Porter, *J. Electroanal. Chem.*, 2006, **591**, 189–200.
10 A. J. Bergren and M. D. Porter, *J. Electroanal. Chem.*, 2007, **599**, 12–22.
11 A. J. Bergren, K. D. Harris, F. Deng and R. L. McCreery, *J. Phys.: Condens. Matter*, 2008, **20**, 374117.
12 R. L. McCreery, *Chem. Mater.*, 2004, **16**, 4477–4496.
13 R. L. McCreery, *Anal. Chem.*, 2006, **78**, 3490–3497.
14 R. M. Metzger, *Chem. Phys.*, 2006, **326**, 176–187.
15 J. R. Heath, *Annu. Rev. Mater. Res.*, 2009, **39**, 1–23.
16 A. Vilan, O. Yaffe, A. Biller, A. Salomon, A. Kahn and D. Cahen, *Adv. Mater.*, 2010, **22**, 140–159.
17 H. Haick and D. Cahen, *Acc. Chem. Res.*, 2008, **41**, 359–366.
18 A. Salomon, D. Cahen, S. Lindsay, J. Tomfohr, V. B. Engelkes and C. D. Frisbie, *Adv. Mater.*, 2003, **15**, 1881–1890.
19 K. Moth-Poulsen and T. Bjornholm, *Nat. Nanotechnol.*, 2009, **4**, 551–556.
20 R. E. Holmlin, R. Haag, M. L. Chabinyc, R. F. Ismagilov, A. E. Cohen, A. Terfort, M. A. Rampi and G. M. Whitesides, *J. Am. Chem. Soc.*, 2001, **123**, 5075–5085.
21 A. V. Walker, T. B. Tighe, O. M. Cabarcos, M. D. Reinard, B. C. Haynie, S. Uppili, N. Winograd and D. L. Allara, *J. Am. Chem. Soc.*, 2004, **126**, 3954–3963.
22 Z. Zhu, T. A. Daniel, M. Maitani, O. M. Cabarcos, D. L. Allara and N. Winograd, *J. Am. Chem. Soc.*, 2006, **128**, 13710–13719.
23 F. Anariba, J. K. Steach and R. L. McCreery, *J. Phys. Chem. B*, 2005, **109**, 11163–11172.
24 H. B. Akkerman, P. W. M. Blom, D. M. de Leeuw and B. de Boer, *Nature*, 2006, **441**, 69–72.
25 K. W. Hipps, *Science*, 2001, **294**, 536–537.
26 C. A. Nijhuis, W. F. Reus and G. M. Whitesides, *J. Am. Chem. Soc.*, 2009, **131**, 17814–17827.
27 C. A. Nijhuis, W. F. Reus, J. R. Barber, M. D. Dickey and G. M. Whitesides, *Nano Lett.*, 2010, **10**, 3611–3619.
28 Ryan C. Chiechi, Emily A. Weiss, Michael D. Dickey and George M. Whitesides, *Angew. Chem., Int. Ed.*, 2008, **47**, 142–144.
29 S. Ranganathan, I. Steidel, F. Anariba and R. L. McCreery, *Nano Lett.*, 2001, **1**, 491–494.
30 W. R. McGovern, F. Anariba and R. L. McCreery, *J. Electrochem. Soc.*, 2005, **152**, E176–E183.
31 A. P. Bonifas and R. L. McCreery, *Nat. Nanotechnol.*, 2010, **5**, 612–617.
32 A. M. Mahmoud, A. J. Bergren and R. L. McCreery, *Anal. Chem.*, 2009, **81**, 6972–6980.
33 A. M. Mahmoud, A. J. Bergren, N. Pekas and R. L. McCreery, *Adv. Funct. Mater.*, 2011, DOI: 10.1002/adfm.201002496.
34 S. Ssenyange, H. Yan and R. L. McCreery, *Langmuir*, 2006, **22**, 10689–10696.
35 S. Ranganathan, R. L. McCreery, S. M. Majji and M. Madou, *J. Electrochem. Soc.*, 2000, **147**, 277–282.
36 S. Ranganathan and R. L. McCreery, *Anal. Chem.*, 2001, **73**, 893–900.
37 R. L. McCreery, *Chem. Rev.*, 2008, **108**, 2646–2687.
38 F. Anariba, S. H. DuVall and R. L. McCreery, *Anal. Chem.*, 2003, **75**, 3837–3844.
39 H. Yan and R. L. McCreery, *ACS Appl. Mater. Interfaces*, 2009, **1**, 443–451.
40 L. C. T. Shoute, A. J. Bergren, A. M. Mahmoud, K. D. Harris and R. L. McCreery, *Appl. Spectrosc.*, 2009, **63**, 133–140.
41 H. Tian, A. J. Bergren and R. L. McCreery, *Appl. Spectrosc.*, 2007, **61**, 1246–1253.
42 S. Donner, H.-W. Li, E. S. Yeung and M. D. Porter, *Anal. Chem.*, 2006, **78**, 2816–2822.
43 A. Scott, C. A. Hacker and D. B. Janes, *J. Phys. Chem. C*, 2008, **112**, 14021–14026.
44 H. Liang, H. Tian and R. L. McCreery, *Appl. Spectrosc.*, 2007, **61**, 613–620.
45 A. J. Bergren and R. L. McCreery, *Annu. Rev. Anal. Chem.*, 2011, **4**, 173–195.
46 E. A. Weiss, R. C. Chiechi, G. K. Kaufman, J. K. Kriebel, Z. Li, M. Duati, M. A. Rampi and G. M. Whitesides, *J. Am. Chem. Soc.*, 2007, **129**, 4336–4349.
47 H.-H. Yang and R. L. McCreery, *Anal. Chem.*, 1999, **71**, 4081–4087.
48 S. A. DiBenedetto, A. Facchetti, M. A. Ratner and T. J. Marks, *J. Am. Chem. Soc.*, 2009, **131**, 7158–7168.
49 H. Liu, N. Wang, J. Zhao, Y. Guo, X. Yin, F. Y. C. Boey and H. Zhang, *ChemPhysChem*, 2008, **9**, 1416–1424.
50 M. J. Frisch, G. W. Trucks, H. B. Schlegel, G. E. Scuseria, M. A. Robb, J. R. Cheeseman, J. Montgomery, J. A. T. Vreven, K. N. Kudin, J. C. Burant, J. M. Millam, S. S. Iyengar, J. Tomasi, V. Barone, B. Mennucci, M. Cossi, G. Scalmani, N. Rega, G. A. Petersson, H. Nakatsuji, M. Hada, M. Ehara, K. Toyota, R. Fukuda, J. Hasegawa, M. Ishida, T. Nakajima, Y. Honda, O. Kitao, H. Nakai, M. Klene, X. Li, J. E. Knox, H. P. Hratchian, J. B. Cross, V. Bakken, C. Adamo, J. Jaramillo, R. Gomperts, R. E. Stratmann, O. Yazyev, A. J. Austin, R. Cammi, C. Pomelli, J. W. Ochterski, P. Y. Ayala, K. Morokuma, G. A. Voth, P. Salvador, J. J. Dannenberg, V. G. Zakrzewski, S. Dapprich, A. D. Daniels, M. C. Strain, O. Farkas, D. K. Malick, A. D. Rabuck, K. Raghavachari, J. B. Foresman, J. V. Ortiz, Q. Cui, A. G. Baboul, S. Clifford, J. Cioslowski, B. B. Stefanov, G. Liu, A. Liashenko, P. Piskorz, I. Komaromi, R. L. Martin, D. J. Fox, T. Keith, M. A. Al-Laham, C. Y. Peng, A. Nanayakkara, M. Challacombe, P. M. W. Gill, B. Johnson, W. Chen, M. W. Wong, C. Gonzalez and J. A. Pople, *Gaussian 03*, Gaussian, Inc., Wallingford, CT, 2004.
51 *CRC Handbook of Chemistry and Physics*, ed. D. R. Lide, CRC Press, New York, 76th edn, 1996.

